energies

MDPI

Article

Proportional-Integral Controllers Performance of a Grid-Connected Solar PV System with Particle Swarm Optimization and Ziegler–Nichols Tuning Method

Klemen Deželak [1,*], Peter Bracinik [2], Klemen Sredenšek [1] and Sebastijan Seme [1,3]

[1] Faculty of Energy Technology, University of Maribor, Hočevarjev trg 1, 8270 Krško, Slovenia; klemen.sredensek@um.si (K.S.); sebastijan.seme@um.si (S.S.)
[2] Faculty of Electrical Engineering and Information Technology, University of Zilina, Univerzitna 8215/1, 010 26 Zilina, Slovakia; peter.bracinik@uniza.sk
[3] Faculty of Electrical Engineering and Computer Science, University of Maribor, Koroška Cesta 46, 2000 Maribor, Slovenia
* Correspondence: klemen.dezelak@guest.um.si

Abstract: This paper deals with photovoltaic (PV) power plant modeling and its integration into the medium-voltage distribution network. Apart from solar cells, a simulation model includes a boost converter, voltage-oriented controller and LCL filter. The main emphasis is given to the comparison of two optimization methods—particle swarm optimization (PSO) and the Ziegler–Nichols (ZN) tuning method, approaches that are used for the parameters of Proportional-Integral (PI) controllers determination. A PI controller is commonly used because of its performance, but it is limited in its effectiveness if there is a change in the parameters of the system. In our case, the aforementioned change is caused by switching the feeders of the distribution network from an open-loop to a closed-loop arrangement. The simulation results have claimed the superiority of the PSO algorithm, while the classical ZN tuning method is acceptable in a limited area of operation.

Keywords: photovoltaic power plant; optimization; PI controllers; distribution system

Citation: Deželak, K.; Bracinik, P.; Sredenšek, K.; Seme, S. Proportional-Integral Controllers Performance of a Grid-Connected Solar PV System with Particle Swarm Optimization and Ziegler–Nichols Tuning Method. *Energies* **2021**, *14*, 2516. https://doi.org/10.3390/en14092516

Academic Editor: Teuvo Suntio

Received: 30 March 2021
Accepted: 24 April 2021
Published: 27 April 2021

1. Introduction

Due to increasing environmental awareness, legal regulations and international agreements that require an improvement of energy efficiency and a decrease of carbon emissions, there is a need to raise the share of renewable energy sources in the total energy balance of the community. Renewable energy sources (such as biomass, water energy, wind energy, solar energy, etc.) continue to set record levels for investment. These sources are known for being an "endless" source of energy that, with correct exploitation, could be able to meet the world's ever-growing needs. So, an ideal energy source should be renewable and should have a minimal effect on the environment. Among the renewable energy sources, solar energy is considered the most encouraging candidate and is expected to be the base of a sustainable energy economy, as sunlight is the most generous resource [1,2].

Solar energy and its related PV power plants, where the system directly converts solar energy into electricity, have become one of the most important renewable energy sources [3,4]. The generated electrical energy depends mainly on solar radiation reaching the PV modules G, the temperature T, as well as the material and the inverter types [5,6]. PV systems are classified into grid-connected and off-grid application varieties. Off-grid PV systems have a big potential for economic application in the unelectrified areas of developing countries. On the other side, grid-connected PV systems use various electronic power devices, mainly the direct current (DC) boost converters and inverters, to convert electricity from DC to alternating current (AC), and afterward supply the produced electricity to the electrical grid [7].

Of course, from a functional point of view, a PV system may face substantial deviations of its output power under changeable weather conditions. They may be responsible for power fluctuations and voltage rises in the system, thus resulting in problems of grid control [8–12]. Grid-connected PV systems based on voltage-oriented control (VOC), with pulse width modulation (PWM) topology, generate some harmonic distortions which can be rectified using an LCL filter. As a filter may cause some resonance peak, it influences the stability of the system; therefore, a proportional-integral (PI) controller is utilized to improve the system stability [9,12].

Several works have concentrated on the control strategy for grid-connected PV systems [13–19], considering a voltage regulation in the distribution system [15], a VAr control strategy with PV inverters in distribution networks to provide VAr support [16] or a control strategy to mitigate the voltage fluctuations [18]. Some of the results indicate that the control strategy is able to operate under the various operating modes of PV systems, while, within a limited area, some of the conditions can be improved even without additional regulators. The aforementioned various operating modes are an excess of PV power generation, normal condition, low or no PV power output or passing clouds [15,16]. An improved, automatic, coordinated voltage control strategy performed by the authors in [18] combines the advantages of several controls which demonstrates a better control performance, especially in extreme environments. Furthermore, different strategies for controlling the distributed generators in terms of a current harmonic compensator [20–22] or unbalanced three-phase loads have been discussed and analyzed [23]. It is challenging to suppress the harmonic content below a pre-set value or to compensate for unbalanced loads [20]. Similarly, a novel energy-management method for a grid-connected PV inverter is investigated. Results indicate that by using this controlling structure, overall power loss diminishes by about 18% [23].

However, in a grid-connected system, a generated resonance peak is often related to the feeder's arrangement, where the feeders in the open-loop arrangement are shifted to closed-loop to upgrade the reliability of the power supply [24–29]. Some earlier works have dealt with upgrading primary feeders from radial and open-loop to a normally closed-loop arrangement, but not in terms of a controlling structure. The contributions were correlated with the voltage profiles, power flows and short-circuit capacities of the feeders under both the tie-breaker normally open or occasionally closed conditions; measurements and the impacts of the upgrading of system type on the distribution system and customers were assessed [24,26–28]. Unlike the aforementioned paper, our research fills some gaps by providing a controlling structure related to both open and closed-loop arrangements of feeders. A proportional gain and integral time constant of the PI controller are set by the ZN tuning method approach and are also used as the design variables of the optimization problem, where their values influence the system feedback. The procedures are performed for both the open-loop as well as closed-loop arrangement of feeders.

2. Model of PV Power Plant

A grid-connected PV system is shown in Figure 1. It is composed of a PV array (solar cells), a boost converter with a maximum power point tracker (MPPT), an inverter with VOC and a transformer (TR). The AC power is delivered to the grid with the help of the LCL filter. The mathematical model of the solar cell, boost converter with MPPT, VOC and LCL filter are briefly described in Sections 2.1–2.3.

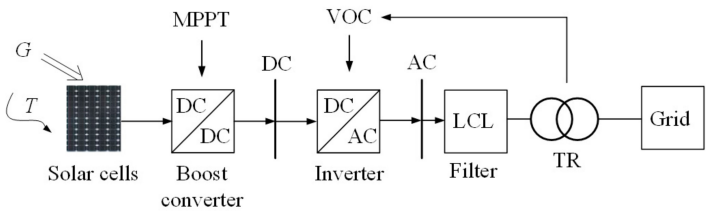

Figure 1. Block diagram of the studied system.

2.1. Solar Cell

Equation (1) represents an important part related to the solar cell model. The diode saturation current I_{sat} and the Boltzmann constant k are involved in the model, where q is the electron charge and Q_{d} is the quality factor. The equivalent circuit of a solar cell is shown in Figure 2 [10], where U is the diode voltage, I_{PH} stands for the photocurrent, I_{D} is the diode current, while parallel R_P and series resistance R_S represent the leakage currents in the diode and the losses related to the connections and the contacts. Symbols G, T and DI stand for the solar radiation level, temperature and diode, respectively, while I_C and U_C are the current and voltage of the solar cell. Equation (1) is usually modified in terms of several solar cells consideration [10,30].

$$I_{\text{D}} = I_{\text{sat}}\left(e^{\left(\frac{qU}{kTQ_{\text{d}}}\right)} - 1\right) \tag{1}$$

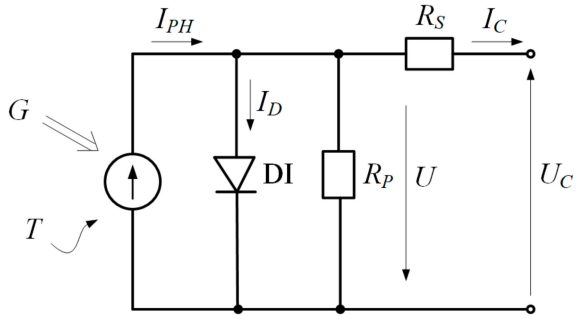

Figure 2. Solar cell equivalent circuit.

2.2. Boost Converter with MPPT

A boost converter is a DC–DC power converter, where an output voltage U_{OUT} is higher than its input voltage U_{INP}. Important boost converter equations and a schematic presentation are shown by Equations (2)–(4) and Figure 3 [31,32]. When the switch (SW) is switched on, the current flows through the inductor L_{BO} and energy is stored in it, while during switch-off the input voltage and the voltage across the inductor are in series. These voltages charge the output capacitor C_{BO} to a voltage higher than the input voltage. In that sense, the key ratings targeted for the converter design are a rated power between 1.5 kW and 6 kW, an input voltage range between 200 V and 600 V, an output voltage of 600 V and an efficiency approximately equal to 98% [33]. Values of L_{BO} and C_{BO} could be defined after the desired inductor current ripple Δi_L, the desired output voltage ripple Δu_{OUT} and minimum switching frequency of boost converter f_S are chosen. At the same time, the input voltage U_{INP} and desired output voltage U_{OUT} should also be prescribed. The first step is to define the duty cycle D (4) for the minimum input voltage and the maximal output current $i_{OUT\text{max}}$ necessary for the application [32]. After that, the values of both L_{BO} and C_{BO} could be calculated by Equations (2) and (3).

$$L_{BO} = \frac{U_{INP}D}{\Delta i_L f_S} \tag{2}$$

$$C_{BO} = \frac{i_{OUT\text{max}}D}{\Delta u_{OUT} f_S} \tag{3}$$

$$\frac{U_{OUT}}{U_{INP}} = \frac{1}{1-D} \tag{4}$$

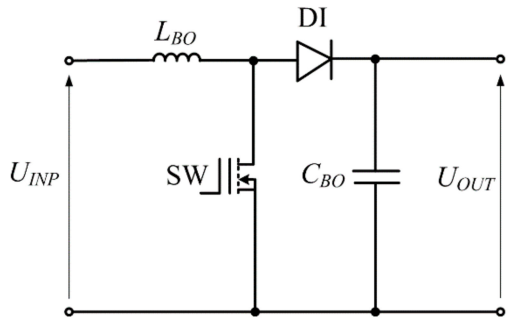

Figure 3. Boost converter equivalent circuit.

The output power of a solar cell is also a function of the voltage and current product. By varying one or both parameters the output power can be maximized. In that sense, the PV system output power can be increased by using a special controller connected to a DC-DC converter for a tracking system. However, the maximum power point (MPP)—at which the complete PV system behaves with maximal efficiency and produces its maximal output power—changes due to the nonlinear characteristic of PV modules, but can be located with MPPT controller [19,34].

2.3. VOC and LCL Filter

This subsection deals with the application of the VOC method to LCL filter-based systems using a set of current measurement blocks. To reduce some higher harmonics close to the switching frequency, occasionally, a high value of input inductance is utilized. However, for implementations over several kilowatts, it becomes too expensive to realize a higher-value filter, while the system's dynamic feedback may become too low. A helpful solution for this problem is to use an LCL filter (Figure 4), with the inductance at the inverter side (L_i), the filter capacitor (C_f) and at the transformer side (L_s). In this manner, a suitable result could be obtained in the range of powers up to hundreds of kVA, while still applying some relatively small values of inductors and capacitors [9,12,35–37].

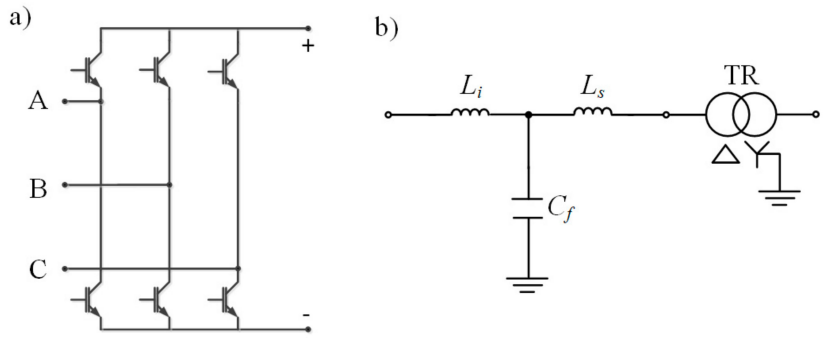

Figure 4. Three-phase voltage source inverter (**a**), and an LCL filter–transformer connection (**b**).

Stability is emphasized with respect to some of the dissimilar ratios of control frequency and resonance frequency of the LCL filters. These are crucial parameters from a control point of view as well as system design. It should be noted that the grid-connected inverter tied with the LCL filter [14,38] is often applied with disable to realize the precise control of a system. Normally, the balanced inverter consists of six switches and forms a three-phase system (Figure 4a). In practice, the asynchronous switching condition for the upper and the lower switches occurs if the gate-driving circuits are not parametrically symmetrical [39]; therefore, the results might show in the form of equalizing currents. This is not the case when the star-connected transformer has a neutral point solidly earthed (Figure 4b, [14]). As presented, the low-voltage winding of the transformer (TR) is con-

nected in delta (Δ), while the high-voltage winding is connected in star (Y) with the neutral point connected directly to the earth.

The basic structure of the VOC strategy is shown in Figure 5. Input variables are the current and voltage measured at the transformer's high-voltage side (I_{TR}, U_{TR}), while the voltage of the DC link U_{DC} is measured and compared to a reference value ($I_{q,ref}$ and $U_{DC,ref}$). The reference of the reactive current component $I_{q,ref}$ is set to 0, thereby seeking a unity power factor. Within transformation, the phase-locked loop (PLL) is used to determine the angle of transformation from three-phase voltages. The grid voltage is transformed in the dq coordinates system, while its output generates commanded voltage source control (VSC) voltages. Such an approach allows the full use of the advantages of PI controllers [19,40]. After backward transformation, the three voltages are delivered to PWM, which generates switching signals for an inverter [40,41].

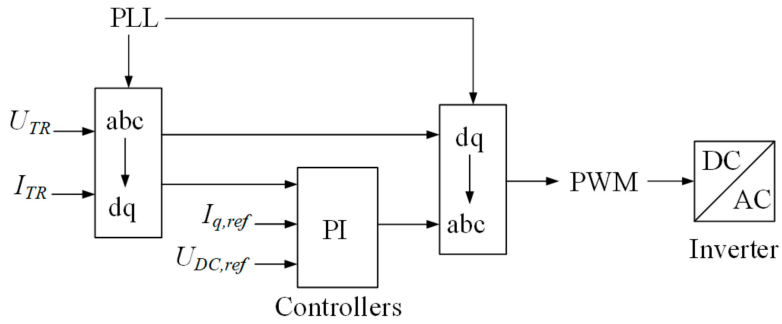

Figure 5. Schematic presentation of applied VOC.

Procedures for the controller's parameters determinations are based on different methods, such as the Ziegler–Nichols method or even on the optimization algorithms applications [9,13,19,34,42–44]. Both procedures are used in this paper.

3. Open and Closed-Loop Operation

The analyzed medium-voltage network is presented in Figure 6. It includes a substation with two 110 kV/20 kV transformers TR I and TR II and two feeders (Feeder 1 and 2) supplied by a high-voltage (HV) network. Measurement points are denoted by M, SW is a switch and MVL stands for the medium-voltage line, while Ld and RS stand for the load and a renewable source of energy. The voltages and currents are studied at the low-voltage side of the transformers. The proposed scheme was chosen because a various specter of measurements has been performed with it in the past [19,26,27,29]. The analyzed medium-voltage network works well, even in the case of some experiments on different combinations of loads and renewable sources of energy [19].

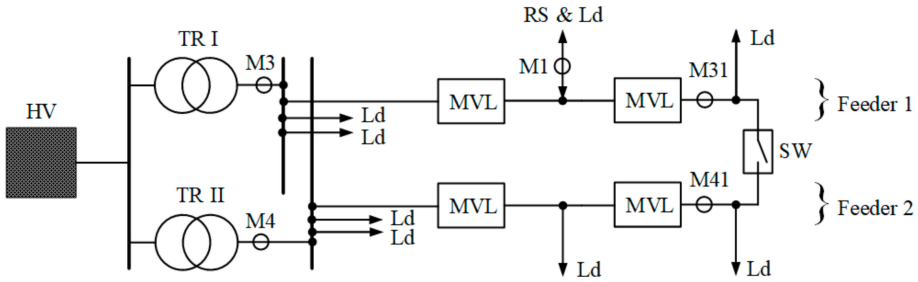

Figure 6. Schematic presentation of discussed medium-voltage network.

In general, a system, apart from electrical sources, involves essential dynamic properties: a capacitance (*C*) as a property of a device to store electrical charges, an inductance (*L*) as a property of a current-carrying conductor that generates a magnetic field around the

conductor and resistance (R) as a measure of the opposition to the current flow. The current, for a particular set of R, L and C, depends on source frequency and the total resistance of the circuit. The current first increases and reaches the maximum value and then decreases with source frequency. The particular value of frequency f, for which the current I reaches the maximum, is called resonance frequency (Figure 7); when this occurs, the circuit is termed a resonance circuit.

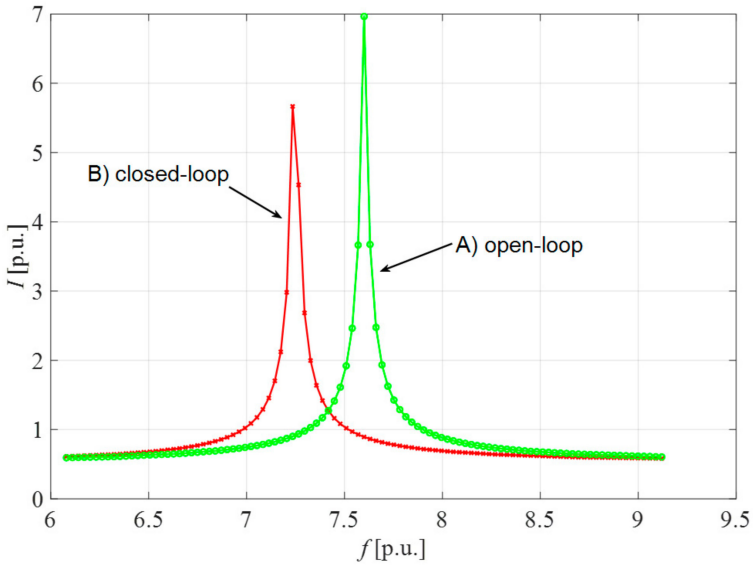

Figure 7. Resonance frequency for the open (A) and closed-loop (B) arrangement.

The feeders in the open-loop arrangement are occasionally modified to the closed-loop arrangement to curtail the power losses generated by an electric power transmission, to upgrade voltage profiles in the feeders with the distributed generation or to increase the power quality and reliability of the power supply [24,29]. Since the total system resistance is dependent on the resistance inserted directly into the network, it could be found that when feeders in the open-loop arrangement are modified to the closed-loop arrangement, that the current through the circuit is changed. In a changed arrangement there becomes a new frequency point where the inductive reactance of the inductors becomes equal in value to the capacitive reactance of the capacitors.

4. Controller Tuning

The PI controller generates an output signal $y(t)$ proportional to both input signal $x(t)$ and integral part (5).

$$y(t) = K_{\mathrm{p}} x(t) + K_{\mathrm{i}} \int x(t) \tag{5}$$

After the reference signal is compared to the actual one, an error signal is contributed to the PI control [33,41]. By choosing an integral (K_{i}) and proportional gain (K_{p}), the desired response can be fulfilled. The process of choosing a controller parameter to match some particular performance specification is known as controller tuning. The suitable values of PI controllers were often set by trials–errors-based proceedings, while ZN suggested that guides for tuning PI controllers are found in the experimental step response. This non-systematic and hard action becomes more difficult and time-consuming, particularly in complex applications. So, the formulation of controller tuning as an optimization problem is a promising resolution.

First, for obtaining the closed-loop performance parameters with PI control, the gain parameters are required where the ZN reaction curve method is applied. Likewise, a step response in the expression of an S-shaped curve in Figure 8 is produced for the PV

system, where the solar radiation is stepped from 0 to 250 W/m^2 (so-called lower-tuning ZN procedure (A)) and from 0 to 500 W/m^2 (higher-tuning ZN procedure (B)), respectively.

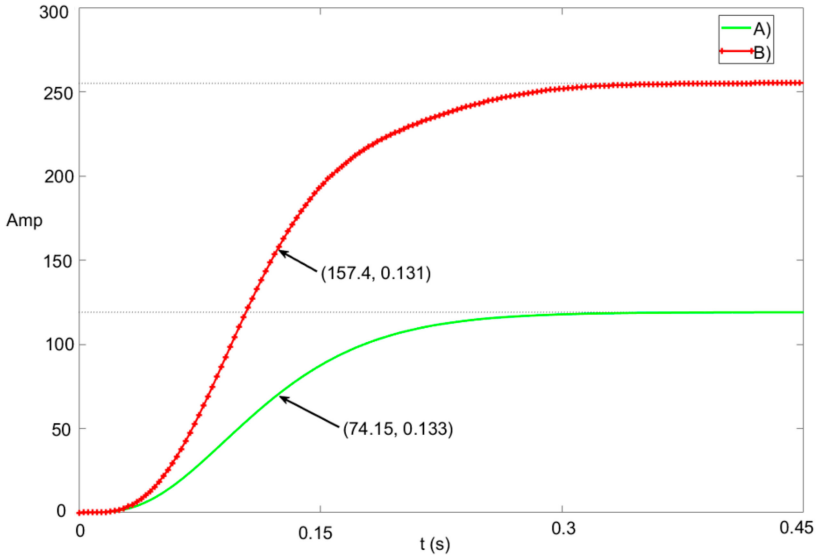

Figure 8. Process variable for solar radiation stepped from 0 to 250 W/m^2 (A) and from 0 to 500 W/m^2 (B).

The time constant is determined from Figure 8 by drawing a tangent from the point of inflection of the curve to cross with the x-axis. The time difference to the point where the curve is at 63% of its ending value (both marked points) is defined as the time constant and has values of 0.133−0.029 = 0.104 s and 0.131−0.029 = 0.102 s, respectively. The time delay (0.029 s), as a difference between the areas where the step appears and the process variable starts to rise, together with the change in process variable (Figure 8) resulted in a critical gain. Finally, the key proportional and integral parameters can be defined by using the settings suggested by the ZN method.

Second, both integral and proportional gains of the PI controller are set as the essential variables inside of the optimization process. In this paper, an application of the Particle Swarm Optimization (PSO)-based PI control strategy is suggested to upgrade the dynamic performance of the analyzed PV systems [19,34]. The optimization procedure is performed once at the beginning of the operation. It is initialized with a population of random solution particles that are linked with a velocity v and position s. In this sense, the solution particles fly through the search area with velocities that are dynamically balanced within a process. All of the solution particles have objective values evaluated by the objective function. The solution particle's condition is modified according to the next three principles [34]:

(1) to hold its inertia;
(2) to adjust the solution particles' position according to its most optimal position;
(3) to adjust the solution particles' position according to the swarm's most optimal position.

So, the individual particles update their velocity $v_{\mathrm{i,new}}$ by the velocity (Equation (6)) where i is the number of particles, $v_{\mathrm{i,old}}$ represents the old velocity, while $P_{\mathrm{best,i}}$ and G_{best} denote the best solution of particle i and the best solution of all particles at a certain point. Coefficients c_1, c_2 are the acceleration parameters and R_1, R_2 are the random numbers distributed between 0 and 1. In our case, the old position of the particles $s_{\mathrm{i,old}}$ is adjusted according to an integral and proportional gain of the PI controller as shown in [19].

$$v_{\mathrm{i,new}} = v_{\mathrm{i,old}} + c_1 R_1 (P_{\mathrm{best,i}} - s_{\mathrm{i,old}}) + c_2 R_2 (G_{\mathrm{best}} - s_{\mathrm{i,old}}) \quad (6)$$

Afterward, the position of each particle $s_{i,new}$ will be updated according to (7), [13].

$$s_{i,new} = f(s_{i,old}, v_{i,new}) \quad (7)$$

5. Results and Discussion

The procedure described in previous sections was applied on a 100 kW PV power plant, where a 100 kW, 0.24/20 kV output transformer was used [19]. Within the procedure (Δu_{OUT} = 2%, f_S = 4000 Hz, Δi_L = 3%, U_{INP}/U_{OUT} = 250 V/500 V), L_{BO} = 3.68 mH, C_{BO} = 589.5 µF and all of the filter parameters L_i = 0.1833 mH, L_s = 0.0916 mH and C_f = 276.3 µF were set, while with the ZN reaction curve method and PSO procedure [19] the parameters of PI controllers were determined. In the case of the ZN reaction curve method, both lower and higher tuning ZN procedures were applied inside of the calculations. For example, results obtained by the lower Ziegler–Nichols procedure were tested with the step responses on two different solar radiation (G = 400 and 800 W/m^2, Figure 9a) levels, where results are presented in Figure 9b,c (G = 400 W/m^2 (A) and G = 800 W/m^2 (B)). In this manner, MPPT currents i_{MPPT}, and powers P_1 at the measurement point M1 (Figure 6) are shown. Better results are obtained for the lower value of solar radiation G = 400 W/m^2 since the ZN procedure is set for the lower radiation step (Figure 8).

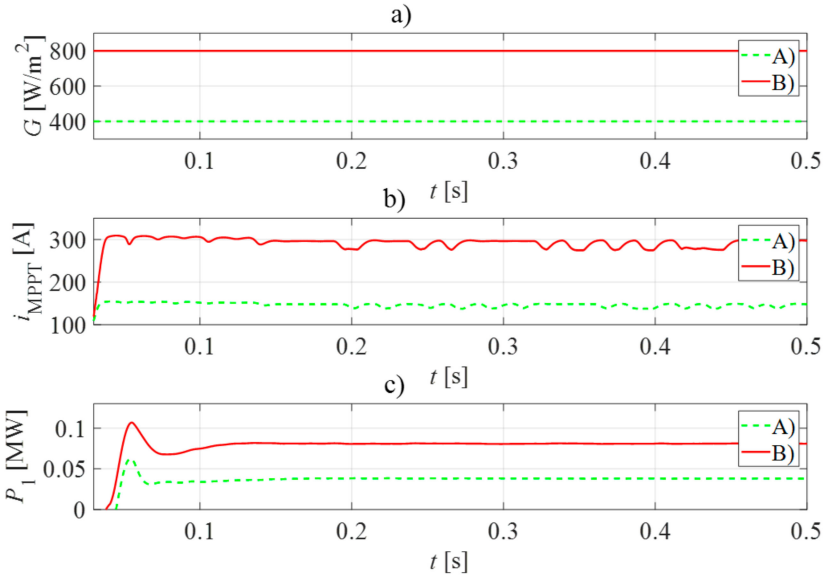

Figure 9. Time-dependent MPPT currents i_{MPPT} (**b**), and powers P_1 (**c**) for the lower-tuning ZN procedure (for two different solar radiations G = 400 W/m^2 (A) and G = 800 W/m^2 (B)—(**a**).

Results obtained by both ZN and PSO methods, within the same computational time, are presented in Figures 10–15. During calculations, the solar radiation G changed on the way presented in Figure 10a, where a positive and negative change of G is triggered in higher and lower specters of solar radiation. Five different powers (P_1, P_3, P_{31}, P_4 and P_{41}) are observed for five different medium-voltage network points (M1, M3, M31, M4 and M41) (Figure 6). Results are presented for the medium-voltage feeders in the open-loop arrangement, as well as the changes to the closed-loop arrangement by an appropriate SW position (Figure 6). Figures 13–15 demonstrate that in the case of the ZN method, both the lower-tuning (LT) and higher-tuning ZN procedures (HT) were compared.

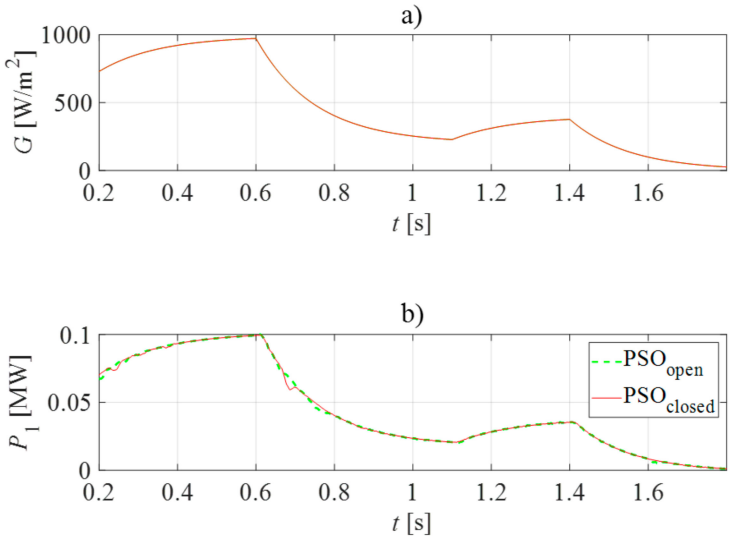

Figure 10. Solar radiation G (**a**) and the output power of PV power plant P_1 (**b**) (PSO method).

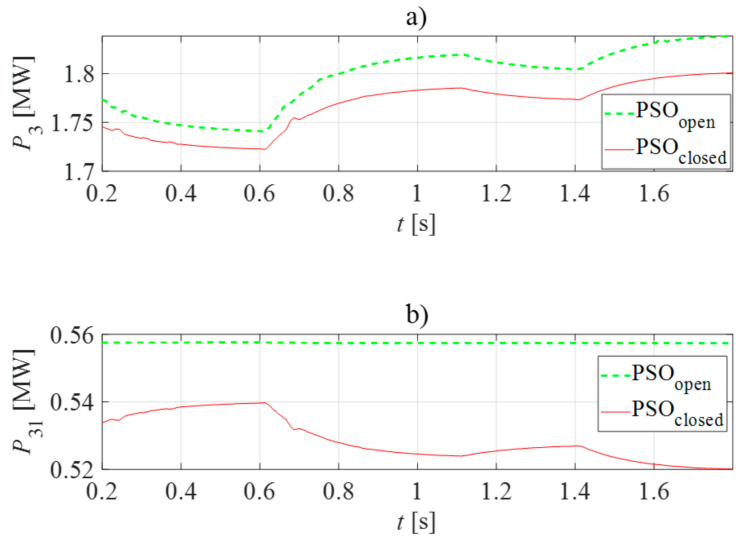

Figure 11. Powers observed at M3 (**a**) and M31 (**b**) points (PSO method).

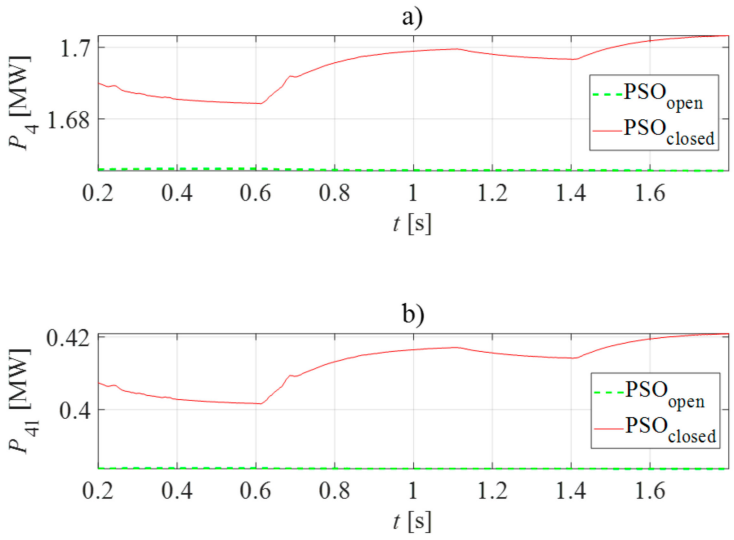

Figure 12. Powers observed at M4 (**a**) and M41 (**b**) points (PSO method).

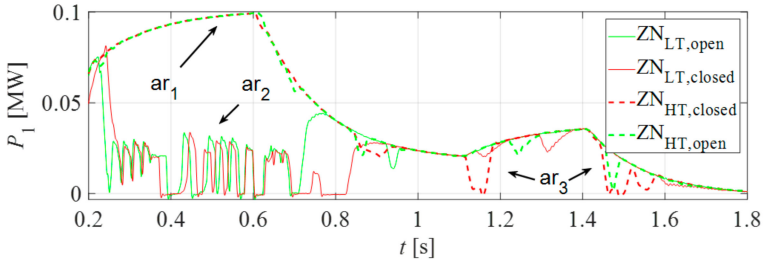

Figure 13. The output power of PV power plant P_1 (ZN method).

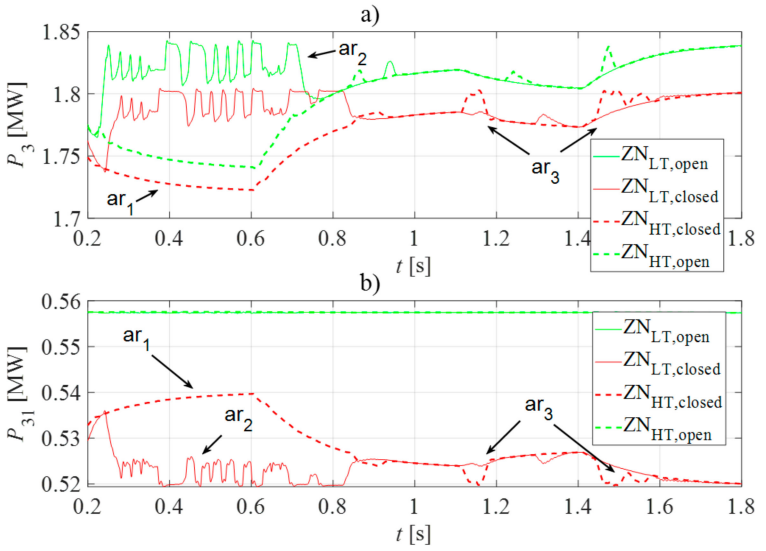

Figure 14. Powers observed at M3 (**a**) and M31 (**b**) points (ZN method).

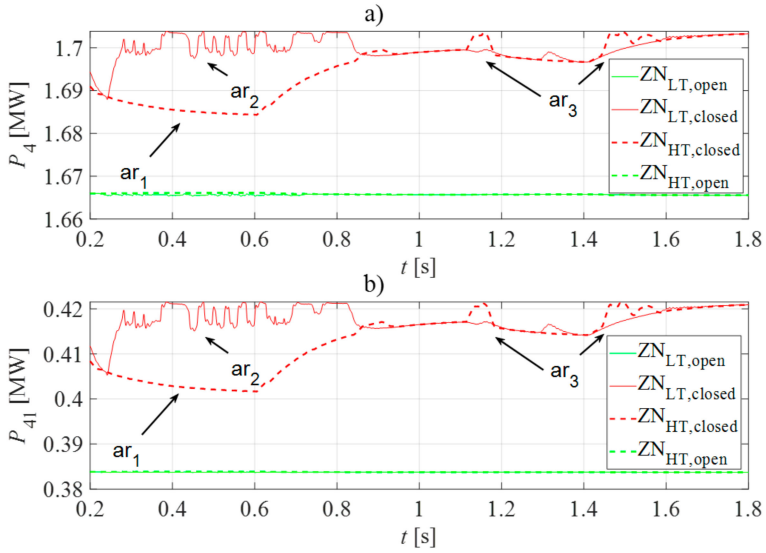

Figure 15. Powers observed at M4 (**a**) and M41 (**b**) points (ZN method).

In general, it is obvious that in the case of higher solar radiation the power at points M3 and M4 (Figure 6) was lower, where part of the energy for the upper feeder (Feeder 1, Figure 6) is delivered from the PV power plant. It is clear that some of the provided results obtained by the ZN method are highly unreliable (low agreement with the ideal values—ar_2), especially in the case of solar radiation levels higher than 500 W/m^2. Otherwise, the results obtained by the PSO gave some highly acceptable results, even with the agreement

higher than 99% (Table 1). In Table 1, ZN—LT and ZN—HT stand for the lower-tuning and higher-tuning ZN procedures, respectively. Results of the agreement to the ideal responses are worse for the applied lower-tuning ZN procedure (under 60%), while higher-tuning ZN procedures are mainly acceptable (above 90%), but still lower in comparison to PSO results. At the same time, it is clear that the agreement results for the closed-loop arrangement are lower than for the open-loop arrangement, while not the case for PSO results, so the procedure could be acceptable in general.

Table 1. The agreement [%] related to the ideal values—results for the complete specter of solar radiation levels.

PSO	ZN—HT	ZN—LT
99.67 [1]	97.02 [1]	58.36 [1]
99.12 [2]	93.31 [2]	56.01 [2]

[1] Open-loop arrangement, [2] closed-loop arrangement.

There is a question, related to Figures 13–15 and ZN results in Table 1, about agreement values for the partly observed solar radiation levels. To obtain an answer, the upper and lower specter of solar radiation levels were used (Tables 2 and 3). In this sense, the limit value of solar radiation was set to 500 W/m^2. The results obtained by ZN—HT and ZN—LT were higher than 90% for the lower specter of solar radiation levels (ar_1 and ar_3), while results for the upper specter of solar radiation levels could be highly unacceptable in the case of ZN—LT (41.25 and 38.20%).

Table 2. The agreement [%] related to the ideal values—results for the upper specter of solar radiation levels.

PSO	ZN—HT	ZN—LT
99.48 [1]	97.60 [1]	41.25 [1]
98.87 [2]	96.54 [2]	38.20 [2]

[1] Open-loop arrangement, [2] closed-loop arrangement.

Table 3. The agreement [%] related to the ideal values—results for the lower specter of solar radiation levels.

PSO	ZN—HT	ZN—LT
99.80 [1]	96.55 [1]	97.44 [1]
99.80 [2]	91.31 [2]	97.80 [2]

[1] Open-loop arrangement, [2] closed-loop arrangement.

6. Conclusions

In this paper, the specific PV power plant model was included within the medium-voltage distribution network as a part of the distribution network during radial and closed-loop operations. So, in the case of available solar radiation, part of the energy for the loads was delivered from the PV power plant. The LCL filter represents an important part of the model, with its main drawback of offering resonance peaks at the resonant frequency, which could make the system unstable. At the same time, the PI controller is commonly used to control the converter because of its good performance, but at the same time, it also has the drawback of not effectively controlling if there is a change in the parameters of the system. In our case, the aforementioned change is caused by switching from the open-loop to the closed-loop arrangement. Time responses of a system with different PI controller-tuning methods show that a PSO-based approach has a great effect on system performance. An additional comparison of the classical Ziegler–Nichols methods shows that the results are partly comparable with those obtained by an aforementioned PSO-based tuning approach but with less computational complexity and a remarkable reduction of the

design time (shorter calculation and simulation times, less complicated programming, less laborious to implement, etc.) and resources (different licensing programs, development tools, etc.). The simulation results have claimed the superiority of the PSO algorithm to systematically tune the PI controllers, while classical Ziegler–Nichols approaches are acceptable mainly in a limited area. In general, PSO tuning leads to better performance with a reduced amplitude peak of overshoot. It is obvious that for the closed-loop arrangement of feeders, the agreement results of the classical approaches are lower than those of the open-loop arrangement, while also not the case for PSO results, so the procedure could be generally acceptable.

Author Contributions: Conceptualization, K.D. and P.B.; methodology, K.D.; software, K.D. and P.B.; validation, K.D., P.B. and S.S.; formal analysis, K.D.; investigation, K.S.; resources, S.S.; data curation, K.D. and P.B.; writing—original draft preparation, K.D.; writing—review and editing, P.B.; visualization, K.S.; supervision, S.S.; project administration, S.S.; funding acquisition, S.S. All authors have read and agreed to the published version of the manuscript.

Funding: This research received no external funding.

Conflicts of Interest: The authors declare no conflict of interest. The funders had no role in the design of the study; in the collection, analyses, or interpretation of data; in the writing of the manuscript, or in the decision to publish the results.

Nomenclature

PV	photovoltaic
LCL	applied filter
PSO	Particle Swarm Optimization
ZN	Ziegler–Nichols
PI	Proportional-Integral
DC	direct current
AC	alternating current
VOC	voltage-oriented control
PWM	pulse-width modulation
MPPT	maximum power point tracker
TR	transformer
DI	diode
SW	switch
MPP	maximum power point
Δ	winding of transformer connected in delta
Y	winding of transformer connected in star
PLL	phase-locked loop
VSC	voltage source control
HV	high-voltage
M	measurement point
MVL	medium-voltage line
Ld	load
RS	renewable source
LT	lower-tuning
HT	higher-tuning

Quantities used in equations:

I_D	diode current
I_{sat}	diode saturation current
q	electron charge
U	diode voltage
Q_d	quality factor
k	Boltzmann constant
T	temperature
L_{BO}	inductor (boost converter)
U_{OUT}	output voltage

L_{BO}	inductor (boost converter)
U_{OUT}	output voltage
U_{INP}	input voltage
Δi_L	desired inductor current ripple
f_S	switching frequency of boost converter
D	duty cycle
C_{BO}	capacitor (boost converter)
Δu_{OUT}	desired output voltage ripple
i_{OUTmax}	maximal output current
$x(t)$	input signal
$y(t)$	output signal
K_i	integral part (controller)
K_p	proportional gain (controller)
V	velocity
s	position
i	number of particles
R_1, R_2	random numbers (PSO)
c_1, c_2	acceleration parameters (PSO)
$P_{best,i}$	best solution of particle *i*
G_{best}	best solution of all particles

References

1. Ma, T.; Yang, H.; Lu, L. Solar photovoltaic system modeling and performance prediction. *Renew. Sustain. Energy Rev.* **2014**, *36*, 304–315. [CrossRef]
2. Muneer, T.; Asif, M.; Kubie, J. Generation and transmission prospects for solar electricity: UK and global markets. *Energy Conv. Manag.* **2003**, *44*, 35–52. [CrossRef]
3. Ahmad, G.E.; Hussein, H.M.S.; El-Ghetany, H.H. Theoretical analysis and experimental verification of PV modules. *Renew. Energy* **2003**, *28*, 1159–1168. [CrossRef]
4. Ghani, Z.A.; Hannan, M.A.; Mohamed, A. Investigation of three-phase grid-connected inverter for photovoltaic application. *Electr. Rev.* **2012**, *7*, 8–13.
5. Tyagi, V.; Rahim, N.A.; Rahim, N.; Jeyraj, A.; Selvaraj, L. Progress in solar PV technology: Research and achievement. *Renew. Sustain. Energy Rev.* **2013**, *20*, 443–461. [CrossRef]
6. El-Adawi, M.K.; Al-Nuaim, I.A. The temperature functional dependence of VOC for a solar cell in relation to its eciency new approach. *Desalination* **2007**, *209*, 91–96. [CrossRef]
7. Ellabban, O.; Abu-Rub, H.; Blaabjerg, F. Renewable energy resources: Current status, future prospects and their enabling technology. *Renew. Sustain. Energy Rev.* **2014**, *39*, 748–764. [CrossRef]
8. Selvaraj, J.; Nasrudin, A.R. Multilevel inverter for grid-connected PV system employing digital PI controller. *IEEE Trans. Ind. Electron.* **2006**, *56*, 149–158. [CrossRef]
9. Negi, P.; Pal, Y.; Leena, G. Stability enhancement of grid connected PV system using model reference adaptive controller. *J. Inf. Opt. Sci.* **2020**, *41*, 461–473.
10. Eltawil, M.A.; Zhao, Z. Grid-connected photovoltaic power systems: Technical and potential problems—A review. *Renew. Sustain. Energy Rev.* **2010**, *14*, 112–129. [CrossRef]
11. Ro, K.; Rahman, S. Two-loop controller for maximizing performance of a grid-connected photovoltaic-fuel cell hybrid power plant. *IEEE Trans Energy Conv.* **1998**, *13*, 276–281.
12. Hato, M.M.; Bouallegue, S. Whale Optimization Algorithm for Active Damping of LCL-Filter-Based Grid-Connected Converters. *Int. J. Renew. Res.* **2019**, *9*, 986–996.
13. Kabalcı, E. Review on novel single-phase grid-connected solar inverters: Circuits and control methods. *Solar Energy* **2020**, *198*, 247–274. [CrossRef]
14. Khalifa, A.S.; El-Saadany, E.F. Control of three phase grid connected photovoltaic power systems. In Proceedings of the 14th International Conference on Harmonics and Quality of Power (ICHQP), Bergamo, Italy, 26–29 September 2010.
15. Pyo, G.C.; Kang, H.W.; Moon, S.I. A new operation method for grid-connected PV system considering voltage regulation in distribution system. In Proceedings of the Power and Energy Society General Meeting-Conversion and Delivery of Electrical Energy in the 21st Century, Pittsburgh, PA, USA, 20–24 July 2008.
16. Alam, M.J.E.; Kashem, M.M.; Sutanto, D. A multi-mode control strategy for VAr support by solar PV inverters in distribution networks. *IEEE Trans. Power Syst.* **2014**, *30*, 1316–1326. [CrossRef]
17. Mohamed Hariri, M.H.; Mat Desa, M.K.; Masri, S.; Mohd Zainuri, M.A.A. Grid-Connected PV Generation System—Components and Challenges: A Review. *Energies* **2020**, *13*, 4279. [CrossRef]
18. Qi, Y.; Jia, H. Research on a new voltage control strategy for photovoltaic grid-connected system. In Proceedings of the International Conference on Electrical Machines and Systems, Beijing, China, 20–23 August 2011.

19. Dezelak, K.; Bracinik, P.; Hoger, M.; Otcenasova, A. Comparison between the particle swarm optimisation and differential evolution approaches for the optimal proportional-integral controllers design during photovoltaic power plants modelling. *IET. Renew. Power Gen.* **2016**, *10*, 522–530. [CrossRef]
20. Naderipour, A.; Asuhaimi, M.Z.A.; Bin Habibuddin, M.H.; Miveh, M.R.; Guerrero, J.M. An improved synchronous reference frame current control strategy for a photovoltaic grid-connected inverter under unbalanced and nonlinear load conditions. *PLoS ONE* **2017**, *12*, e0164856. [CrossRef]
21. Mohsen, H.; Karimi, H.; Mokhtari, H. Harmonic and negative-sequence current control in an islanded multi-bus MV microgrid. *IEEE Trans. Smart Grid* **2013**, *5*, 167–176.
22. Qing-Chang, Z.; Hornik, T. Cascaded current–voltage control to improve the power quality for a grid-connected inverter with a local load. *IEEE Trans. Ind. Electron.* **2012**, *60*, 1344–1355.
23. Li, J.; Samavatian, V. Energy management for a grid-connected PV-inverter with a novel power loss mitigation functionality in distributed networks. *Comp. Electron. Eng.* **2020**, *87*, 106769. [CrossRef]
24. Chen, T.H.; Huang, W.T.; Gu, G.C.; Hsu, Y.H.; Guo, T.Y. Feasibility Study of Upgrading Primary Feeders from Radial and Open-Loop to Narmally Closed-Loop Arrangement. *IEEE Trans. Power Syst.* **2004**, *19*, 1308–1316. [CrossRef]
25. Huang, W.T.; Chen, T.H. Assessment of upgrading existing primary feeders from radial to normally closed loop arrangement. In Proceedings of the Transmission and Distribution Conference and Exhibition, Yokohama, Japan, 6–10 October 2002.
26. Štumberger, G.; Deželak, K.; Rošer, M.; Škof, R.; Kastelic, T. Medium-voltage distribution feeders in open-loop and closed-loop arrangement. In Proceedings of the International Conference on Renewable Energies and Power Quality (ICREPQ), Santiago de Compostela, Spain, 28–30 March 2012.
27. Štumberger, G.; Deželak, K.; Rošer, M.; Škof, R.; Kastelic, T. Medium-voltage distribution feeders in closed-loop arrangement–neutral point grounding. In Proceedings of the International Conference on Renewable Energies and Power Quality (ICREPQ), Bilbao, Spain, 20–22 March 2013.
28. Jirapong, P.; Bunchoo, P.; Thararak, P.; Supannon, A.; Burana, S. Effect of upgrading primary feeders from radial to loop arrangement on electrical distribution system performance. In Proceedings of the 12th International Conference on Electrical Engineering/Electronics, Computer, Telecommunications and Information Technology (ECTI-CON), Hua Hin, Thailand, 24–26 June 2015.
29. Deželak, K.; Rošer, M.; Škof, R.; Kastelic, T.; Štumberger, G. The impact of feeders in closed-loop arrangement on harmonic distortion and power losses. In Proceedings of the International Conference on Renewable Energies and Power Quality (ICREPQ), Bilbao, Spain, 20–22 March 2013.
30. Villalva, M.G.; Gazoli, J.R.; Filho, E.R. Comprehensive approach to modeling and simulation of photovoltaic arrays. *IEEE Trans. Power Electron.* **2009**, *24*, 1198–1208. [CrossRef]
31. Valker, G.R.; Senia, P.C. Cascaded DC-DC converter connection of photovoltaic modules. *IEEE Trans. Power Electron.* **2004**, *19*, 1130–1139.
32. Texas Instruments. Basic calculation of a boost converter's power stage. In *Application Report-Low Power DC/DC Application, SLVA372C*; Texas Instruments Incorporated: Dallas, TX, USA, 2009.
33. Agamy, M.S.; Harfman-Todorovic, M.; Elasser, A.; Sabate, J.A.; Steigerwald, R.L.; Jiang, Y.; Essakiappan, S. DC-DC converter topology assessment for large scale distributed photovoltaic plant architectures. In *Energy Conversion Congress and Exposition*; IEEE: Phoenix, AZ, USA, 2011.
34. Sabarish, P.; Sneha, R.; Vijayalakshmi, G.; Nikethan, D. Performance Analysis of PV- Based Boost Converter using PI Controller with PSO Algorithm. *J. Sci. Technol.* **2018**, *3*, 17–24.
35. Liserre, M.; Blaabjerg, F.; Hansen, S. Design and control of an LCL-filter based three-phase active rectifier. *IEEE Trans. Ind. Appl.* **2005**, *41*, 1281–1291. [CrossRef]
36. Ahmed, K.H.; Finney, S.J.; Williams, B.W. Passive filter design for three-phase inverter interfacing in distributed generation. *Electron. Power Qual. Util.* **2007**, *8*, 49–58.
37. Romdhane, M.S.; Naouar, M.W.; Belkhodja, I.S.; Monmasson, E. Robust active damping methods for LCL filter-based grid-connected converters. *IEEE Trans. Power Electron.* **2017**, *32*, 6739–6750. [CrossRef]
38. Tang, Y.; Loh, P.C.; Wang, P.; Choo, F.H.; Gao, F. Exploring inherent damping characteristic of LCL-filters for three-phase grid-connected voltage source inverters. *IEEE Trans. Power Electron.* **2011**, *27*, 1433–1443. [CrossRef]
39. Wang, Z.; Zeng, H.; Sarlioglu, B. Analysis of Modulation Schemes for Balanced Inverter. In Proceedings of the Transportation Electrification Conference & Expo (ITEC), Chicago, IL, USA, 23–26 June 2020.
40. Antoniewicz, P. Predictive Control of three Phase AC/DC Converters. Ph.D. Thesis, Faculty of Electrical Engineering, Warsaw University of Technology, Warsaw, Poland, 2009.
41. Kazmierkowski, M.P.; Malesani, L. Current control techniques for three-phase voltage-source pwm converters: A survey. *IEEE Trans. Ind. Electron.* **1998**, *45*, 691–703. [CrossRef]
42. Anto, E.K.; Asumadu, J.A.; Okyere, P.Y. PID Control for improving P&O-MPPT performance of a grid-connected solar PV system with Ziegler-Nichols tuning method. In Proceedings of the International Conference on Industrial Electronics and Applications (ICIEA), Hefei, China, 5–7 June 2016.

43. Anula, K.; Rangnekar, S. A review of particle swarm optimization and its applications in solar photovoltaic system. *Appl. Soft Comp.* **2013**, *13*, 2997–3006.
44. Arya, L.D.; Titare, L.S.; Kothari, D.P. Improved particle swarm optimization applied to reactive power reserve maximization. *Int. J. Electr. Power Energy Syst.* **2010**, *32*, 368–374. [CrossRef]